Water Resources Research

RESEARCH ARTICLE
10.1029/2018WR023551

Climate, Landforms, and Geology Affect Baseflow Sources in a Mountain Catchment

Catalina Segura[1], David Noone[2], Dana Warren[3,4], Julia A. Jones[2], Johnathan Tenny[1], and Lisa M. Ganio[5]

[1]Forest Engineering, Resources, and Management, Oregon State University, Corvallis, OR, USA, [2]Geography, College of Earth Ocean and Atmospheric Sciences, Oregon State University, Corvallis, OR, USA, [3]Department of Forest Ecosystems and Society, Oregon State University, Corvallis, OR, USA, [4]Department of Fisheries and Wildlife, Oregon State University, Corvallis, OR, USA, [5]Department of Statistics, Oregon State University, Corvallis, OR, USA

Key Points:
- In an average water year isotope patterns of baseflow reflected an elevational-dependent influence of precipitation and seasonal snowpack
- In a year with low snowpack, baseflow isotope patterns showed greater influence of water stored in colluvial deposits, such as earthflows
- As snowpacks decline, groundwater stored in colluvial deposits and bedrock will have greater influence on spatial patterns of baseflow

Supporting Information:
- Supporting Information S1

Correspondence to:
C. Segura,
segurac@oregonstate.edu

Citation:
Segura, C., Noone, D., Warren, D., Jones, J., Tenny, J., & Ganio, L. (2019). Climate, landforms, and geology affect baseflow sources in a mountain catchment. *Water Resources Research*, *55*. https://doi.org/10.1029/2018WR023551

Received 27 JUN 2018
Accepted 18 APR 2019
Accepted article online 6 MAY 2019

Abstract Baseflow is essential for stream ecosystems and human water uses, particularly in areas with Mediterranean climates. Yet the factors controlling the temporal and spatial variability of baseflow and its sources are poorly understood. Measurements of oxygen and hydrogen isotopic composition ($\delta^{18}O$ and $\delta^{2}H$) were used to evaluate controls on baseflow in the stream network of a 64-km^2 catchment in western Oregon. A total of 607 water samples were collected to contrast baseflow in a year of near average precipitation (2016) to a year with low winter snowpack and subsequent summer drought conditions (2015). Spatial autocorrelation structures and relationships between surface water isotopic signatures and geologic and topographic metrics throughout the network were determined using Spatial Stream Network models. Isotope values varied widely in space and between years, indicating disparate baseflow water sources. During average flow conditions, the spatial variation in $\delta^{18}O$ was primarily related to elevation, reflecting the influence of prior precipitation and input of water from snowmelt at higher elevation. In contrast, during drought conditions, the spatial variation in $\delta^{18}O$ was also related to terrain slope and roughness—proxies for local water storage in deep-seated earthflows and other Quaternary deposits. A prominent spring-fed tributary with high unit baseflow discharge illustrated the importance of subsurface water storage in porous volcanic bedrock. As drought increases in a warming climate, baseflow in mountain catchments may become more dependent on storage in geologic and geomorphic features.

1. Introduction

Baseflow is the primary source of water for streams during periods with little precipitation inputs. Spatial and temporal variability in baseflow determines water availability for aquatic ecosystems and for human uses (Alexander et al., 2007; Freeman et al., 2007; Meyer et al., 2001). Declining snowpack is expected to reduce summer baseflow for much of the western United States and other mountain regions (Mote et al., 2018; Verfaillie et al., 2018). Yet little is known about how such changes will affect spatial and temporal dynamics of baseflow.

Baseflow is influenced by subsurface characteristics and by the amount and form of precipitation inputs, which in turn are controlled by the surface elevational gradient. Soil depth and the permeability of geologic and geomorphic features control deep water storage (Bloomfield et al., 2009; Farvolden, 1963; Jefferson et al., 2006; Tague & Grant, 2004) and water transit times (Hale & McDonnell, 2016; McGuire et al., 2005; Pfister et al., 2017; Tetzlaff et al., 2009). For example, deep-seated earthflows and Quaternary deposits can store and release water on interannual timescales (Swanson & Swanston, 1977). Elevation gradient influence baseflow through orographic effects on precipitation and temperature, which increase precipitation amount as well as snowpack depth and duration at high elevation. In addition, other topographic characteristics such as slope and drainage area are frequently correlated to baseflow dynamics and soil moisture (Beven & Kirkby, 1979; Price, 2011; Woods et al., 1997; Zimmer & Gannon, 2018). Despite widespread recognition of the influence of surface and subsurface factors on baseflow, few studies have attempted to disentangle the effects of surface topography and subsurface characteristics on baseflow dynamics.

The oxygen and hydrogen stable isotope chemistry of water can be used to study hydrologic flow paths by providing mass balance constraints on streamflow that isolate different sources of water contributing to

baseflow. For example, spatial variability in water isotopic composition can be used to distinguish water sources and identify physiographic controls on rainfall-runoff generation processes (Blumstock et al., 2015; Mountain et al., 2015; Nickolas et al., 2017; Ogrinc et al., 2008; Peralta-Tapia et al., 2015; Singh et al., 2016; Soulsby et al., 2000; Tetzlaff & Soulsby, 2008). Baseflow sources have been investigated using water stable isotopes in relatively large (>1,500 km^2), humid systems (Tetzlaff & Soulsby, 2008), and in small (<10 km^2) alpine (Fischer et al., 2015; Zuecco et al., 2018), and temperate catchments (Singh et al., 2016). Although many studies have used spatial sampling of water stable isotopes to detect sources of baseflow, we are not aware of any studies using dense sampling of baseflow in midsize (50–100 km^2) catchments to understand baseflow response to climate variability.

Geostatistical models of stream networks (Peterson & ver Hoef, 2010; ver Hoef & Peterson, 2010) can leverage spatial sampling to create spatially explicit models of isotope signatures, called *isoscapes* (Bowen, 2010; Bowen et al., 2007; Kendall & Coplen, 2001). These geostatistically based isoscape models include autocovariance structures that account for stream-connected distances and network topology as well as landscape and network features, including volume and direction of flowing water. Thus, these models simultaneously describe, and quantitatively explain the drivers of spatial pattern. Network geostatistical models have been applied to infer spatial controls on stream temperature (Isaak et al., 2010, 2014; Steel et al., 2016), fish populations (Isaak et al., 2017), and $^{87}Sr/^{86}Sr$ ratios in streams (Brennan et al., 2016), but they have not been used to infer spatial controls on baseflow.

The goal of this study was to evaluate how elevational gradient and subsurface storage influence spatial patterns of baseflow during a year with an average snowpack and a drought year with little or no snowpack. We took advantage of detailed spatial data on climate, topography, geology, and geomorphology in the H. J. Andrews Experimental Forest, a 64-km^2 mountain catchment, to model the spatial structure of baseflow isotopic composition. We expected the following.

1. The spatial pattern of the isotopic composition of baseflow would be related elevational gradients during average flow conditions, because precipitation amount, precipitation type, and isotopic signature are controlled by orographic processes and this is reflected in the stream water.
2. The spatial pattern of the isotopic composition of baseflow would be more strongly influenced by subsurface storage (i.e., groundwater and storage in low-slope, deep-soil areas) during drought flow conditions because the water stored in these areas and released to baseflow over prolonged dry periods will be a greater fraction of the total flow during dry conditions.

2. Study Area and Methods

This study was conducted in the H. J. Andrews Experimental Forest (hereafter *Andrews Forest*) located in the Western Cascades of Oregon (44.2°N, 122.25°W; Figure 1). The 64-km^2 fifth-order Lookout Creek catchment has four tributaries: Cold, Lookout, Mack, and McRae Creeks (Figure 1). The climate is Mediterranean with wet winters and dry summers. More than 80% of precipitation falls between November and May, and streamflow is dominated by baseflow from July to September. Elevation ranges from 430 to over 1,600 m above sea level. Annual precipitation varies from about 2,300 mm at low elevation to over 3,550 mm at the highest elevation. In most years snowpacks persist from mid-November to the end of June at elevations above 1,000 m, but snow rarely persists more than 2 weeks at lower elevations (Jennings & Jones, 2015; Jones & Perkins, 2010). Vegetation is coniferous forest dominated by Douglas-fir (*Pseudotsuga menziesii*) and western hemlock (*Tsuga heterophylla*) at lower elevation and by noble fir (*Abies procera*) and Pacific silver fir (*Abies amabilis*) at upper elevations. The catchment is underlain by multiple rock types of volcanic origin (Figure 1). Ridges are underlain by Miocene lava flows, which have relatively high porosity, while lower elevation areas are underlain by ash flows, air fall tuffs, and alluvial tuffaceous sediments. Some areas consist of steep slopes with shallow soils, while others are associated with deep-seated, slow-moving earthflows and have relatively low gradient slopes and high roughness (Swanson & James, 1975, Figure 1).

2.1. Sampling of Precipitation and Surface Water

Composite precipitation samples were collected between November 2014 and November 2016 at two meteorological stations (Figure 1). Samples were collected weekly at PRIMET (at 430 m, $n = 83$) and at 3-week intervals at H15MET (at 922 m, $n = 30$). The precipitation-sampling collectors meet International

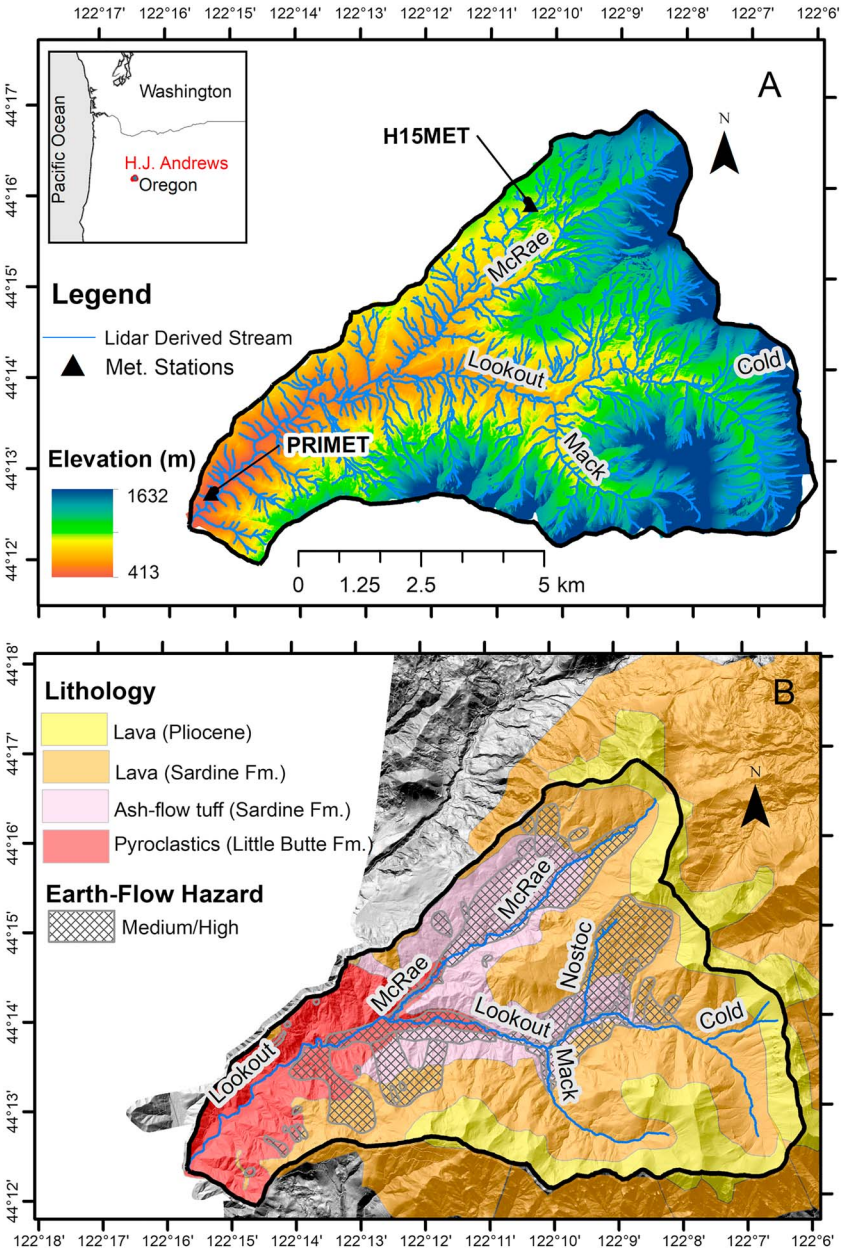

Figure 1. (a) Elevation and (b) geology (Swanson, 2005; Walker & MacLeod, 1991) in the Lookout Creek catchment in the Andrews Forest. Medium and high earthflow hazard areas (Swanson, 2013) are indicated.

Atomic Energy Agency (IAEA) recommendations to prevent evaporation (Groning et al., 2012; Nickolas et al., 2017). Precipitation samples included snow, which was collected in plastic bags and thawed at room temperature before isotopic analysis.

Surface water was sampled over the entire mainstream network of the Andrews Forest on three sampling campaigns during baseflow conditions: July–September 2015, June 2016, and September 2016. Each campaign was completed within an 8-day period during which there was little streamflow variation (coefficient of variation in discharge at Lookout Creek was <9%). Although in 2015 the samples in McRae Creek were collected over a single week, 2 months prior to samples in other locations, the isotopic composition of baseflow on a single sampling location in McRae Creek did not vary over the 2-month period (range between −10.64‰ and −10.56‰ for $\delta^{18}O$; p value of one-way analysis of variance = 0.3). A total of 607 grab samples was obtained: 168 samples in 2015, 238 samples in June 2016, and 201 samples in September 2016. In each

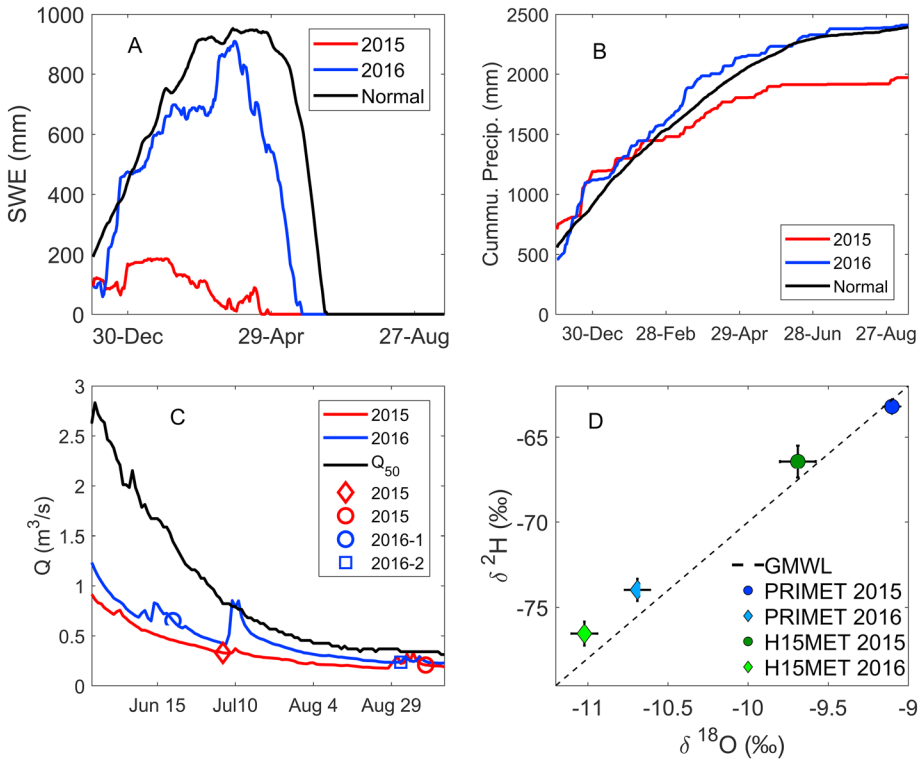

Figure 2. (a and b) Snow water equivalent (SWE) and cumulative precipitation for 2015, 2016, and 30-year Normal at a nearby SNOTEL station (McKenzie). (c) Daily discharge at Lookout Creek (USGS No. 14161500) in 2015 and 2016 and median discharge (Q_{50}) between 1949 and 2017. Sampling times are also indicated. (d) Volume-weighted mean $\delta^{18}O$ and $\delta^{2}H$ for 2015 (Nov 2014-Nov 2015) and 2016 (Nov 2015–Nov 2016) indicated significantly enriched (higher ^{18}O and ^{2}H) precipitation values in the dryer and warmer Nov 2014–Nov 2015 period; error bars represent weighted standard errors.

campaign, samples were collected at ~ 100-m intervals over a stream length of 24.9 km (2015), 39.7 km (June 2016), and 30.0 km (September 2016) in the second- to fifth-order streams of Cold, Lookout, Mack, and McRae Creeks (Figure 1). Locations were recorded using a Garmin 30x Global Positioning System-GPS unit (accuracy 3 m). The stream distance surveyed in 2015 was shorter than in 2016 due to a more contracted network and logistical constraints in accessing some sites.

The three surface water sampling campaigns represent different hydrologic conditions, based on long-term flow records (Daly & McKee, 2016). The 2015 sampling period represented some of the lowest baseflow conditions on record, whereas the 2016 sampling periods represented near average early baseflow (June) and late baseflow (September) conditions. In 2015, mean monthly air temperature was up to 3.9 °C higher and precipitation and snow water equivalent were lower than in 2016 (Figure 2). In the 2015 water year, mean daily discharge in Lookout Creek (United States Geological Survey gauge No. 14161500) was the seventh lowest, whereas in 2016 it was the nineteenth lowest, in the 59-year record. Relative to the 59-year record of daily flows, daily streamflow in June and September was below the 5th percentile during the 2015 sampling (Kaylor et al., 2019) and below the 10th percentile during the sampling in September 2016, whereas daily streamflow during the sampling in June 2016 roughly corresponds to the 50th percentile for July 15 (Figure 2c). Therefore, we refer to the June and September 2016 sampling period as *average* and the 2015 period as *drought* conditions. All precipitation and grab samples were collected in 20-mL borosilicate glass vials with conical inserts and capped without headspace in order to prevent isotopic fractionation. Samples were stored in dark, cool (<15 °C) conditions and analyzed at the Watershed Processes Laboratory of Oregon State University.

2.2. Isotopic Analysis

Water stable isotopes were measured in a total of 607 stream water and 113 precipitation samples using a cavity ring down spectroscopy liquid and vapor isotopic measurement analyzer (Picarro L2130-*i*, Picarro

Inc, CA). Two internal standards were used to develop calibration equations, and a third standard was used to assess accuracy. All the standards were calibrated against the IAEA primary standards for Vienna Standard Mean Ocean Water (VSMOW; $\delta^{18}O$ = 0.0‰, $\delta^{2}H$ = 0.0‰), Standard Light Antarctic Precipitation ($\delta^{18}O$ = -55.5‰, $\delta^{2}H$ = -427.5‰), and Greenland Ice Sheet Precipitation ($\delta^{18}O$ = -24.76‰, $\delta^{2}H$ = -189.5‰). Precision was 0.21‰ and 0.03‰ for $\delta^{2}H$ and $\delta^{18}O$ based on the comparison of 49 duplicated samples. Assuming uncorrelated errors, the internal precision for deuterium excess, defined as *d-excess*=$\delta^{2}H$-(8* $\delta^{18}O$) (Craig, 1961), was 0.22‰. The accuracy was 0.24 ± 0.0045‰ and 0.06 ± 0.0008‰ for $\delta^{2}H$ and $\delta^{18}O$ based on the comparison of 59 estimated values to a known internal standard.

Isotope values were reported in parts per thousand (‰) deviation relative to VSMOW:

$$\delta = \left(\frac{R_s}{R_{std}} - 1\right) \times 1000 \tag{1}$$

where R_s and R_{std} are the isotope ratio ($^{2}H/H$ or $^{18}O/^{16}O$) in the samples and standard (VSMOW) respectively (Craig, 1961). Values for $\delta^{2}H$, $\delta^{18}O$, and d-excess in precipitation are presented in terms of mean mass weight isotopic composition denoted $\overline{\delta^{18}O_p}$, $\overline{\delta^{2}H_p}$, and $\overline{\text{d-excess}}$ where the overbar represents the precipitation amount weighting, to distinguish them from values for individual samples.

2.3. Data Analysis

2.3.1. Variability in Precipitation and Surface Water Isotopic Composition

We analyzed the temporal and spatial variability of $\delta^{2}H$, $\delta^{18}O$, and d-excess in precipitation and grab samples and compared the isotopic composition of precipitation to the isotopic composition of stream water. The average, variance, and lapse rates of the isotopic composition of baseflow ($\delta^{18}O$, $\delta^{2}H$, and d-excess) were computed for each sampled tributary and each sampling campaign and used to characterize the spatial variability. The relative water contribution of three tributaries (Cold, Mack, and McRae Creeks) to the total baseflow in Lookout Creek at their tributary junctions (Figure 1) was estimated assuming a two-component end-member mixing model. The stream mass balance at each tributary junction in the network was computed from two equations:

$$F_1\left(\delta^{18}O_1\right) + F_2\left(\delta^{18}O_2\right) = \left(\delta^{18}O_i\right) \tag{2}$$

$$F_1 + F_2 = 1 \tag{3}$$

where $\delta^{18}O_i$ is $\delta^{18}O$ for the sample downstream of two tributaries, $\delta^{18}O_1$ and $\delta^{18}O_2$ are the $\delta^{18}O$ values of tributaries 1 and 2, and F_1 and F_2 represent the fractions of the total flow downstream of the two tributaries. The uncertainty in the two-end-member model was propagated (Genereux, 1998), and the calculations were repeated with $\delta^{2}H$ in place of $\delta^{18}O$. The error-weighted average of the fractional contribution obtained with both tracers is presented in the results.

2.3.2. Stream Network Models to Predict Isoscapes

We used Spatial Stream Network (SSN) models to estimate the relative importance of surface topography and subsurface storage on baseflow water sources and to predict baseflow isotopes at the network scale. An SSN model consists of a multiple linear regression model for the mean dependent variable ($\delta^{18}O$) and a model for the variance that accounts for spatial autocorrelation within the network. This model thus avoids bias related to spatial autocorrelation. We fitted models for each sampling campaign considering covariates that describe the influence of orographic effects on precipitation amount and snow storage (both measured by elevation) and the effects of subsurface storage (measured by geology, slope, and topographic roughness) (Table 1). Pairs of covariates that were correlated ($R > 0.6$) were not included in the same model (Table 1). In the models, elevation was included to represent the orographic effects on precipitation amount and form the almost universal observation that precipitation becomes more depleted of heavy isotopes (^{18}O and ^{2}H) with increasing elevation (i.e., rainout effect) due to fractionation during Rayleigh (or Rayleigh like) distillation, that is, progressive isotopic depletion of precipitation as elevation or distance from the original vapor source increases (Araguas-Araguas et al., 2000; Dutton et al., 2005; Wassenaar et al., 2009; Williams & Rodoni, 1997; Yonge et al., 1989). Geologic characteristics (e.g., rock permeability) were used as an indication of potential storage. Models included the percentage of area underlain by lava, which likely has relatively high permeability (Saar & Manga, 2004; Figure 1 and Table 1) and ash-flow tuff, that weathers to

Table 1
Covariates Considered in the Spatial Stream Network Models

Covariate[a]	Scale of influence	Source	Description and range
Effects of surface topography on precipitation amount and on the rainout effect[b]			
Elevation (H)	Landscape	LiDAR[c]	Calculated based in the 1-m LiDAR (H) Range: 412–1230 m
Effects of rock permeability on hydrologic flow paths			
Geology (lava, tmt)	Local		Area underlain by ridge-capping lava (lava) Ranges: 0–100%
	Local		Area underlain Ash-flow tuff (tmt) Ranges: 0–100%
Effects of topography on water storage			
Mean slope (S)	Local	LiDAR[c]	Calculated based in the 1-m LiDAR Range: 4–46°
Mean roughness index (R)[d]	Local	LiDAR[c]	This is a proxy for soil/sedimentary thickness. It is calculated as the standard deviation of the residual topography that is the difference between elevation and the mean elevation calculated over a 5-m window Range: 0.025–0.26°

[a]Correlated variables were not considered simultaneously in the models: Area underlain by ridge-capping lava versus ash-flow tuff ($R = -0.64$); slope versus roughness ($R = 0.66$), and area underlain by ridge-capping lava and elevation ($R = 0.80$). [b]Rainout effect occurs due to fractionation during Rayleigh distillation with progressive isotopic depletion of precipitation as elevation or distance from the original vapor source increases (Araguas-Araguas et al., 2000; Dutton et al., 2005; Wassenaar et al., 2009; Williams & Rodoni, 1997; Yonge et al., 1989). [c]Spies (2016). [d]Cavalli et al. (2008).

low-permeability clays and is thus associated with deep-seated slow-moving earthflows (Taskey et al., 1978). Models also included topographic characteristics (slope and roughness). Slope angle and surface roughness are often used to indicate variability in soil depth (McKenzie & Ryan, 1999; Patton et al., 2018; Pelletier et al., 2016). Low slope and relatively high roughness are characteristic of deep, slow-moving earthflows in the Andrews Forest, which may store water for long periods (Swanson & Swanston, 1977).

The influence of covariates on the mean $\delta^{18}O$ in the five tributaries—Cold, upper Lookout (above Cold Creek), Lookout (below Cold Creek), Mack, and McRae Creeks—was estimated within models that permitted slopes and intercepts to vary among the tributaries (hereafter, *estimation models*). In these models, for each covariate, we considered a model that assumed a common, fixed-effect slope but different fixed-effect intercepts for each tributary, and a model that allowed both the fixed-slope and fixed-effect intercept to vary among tributaries. These models thus allow for different relationships between the mean $\delta^{18}O$ and the covariates for each tributary. Models were developed to predict the mean $\delta^{18}O$ in the entire network including locations for which no samples were collected (hereafter, *prediction models*). These models included a single common slope and intercept throughout the stream network for each covariate as opposed to different slopes or intercepts by tributary because the prediction model includes tributaries that were not sampled. All models were fitted using an Andrews Forest stream network derived from LiDAR (Johnson & Lienkaemper, 2016; Spies, 2016) corrected for topological errors (Peterson & ver Hoef, 2014; ver Hoef & Peterson, 2010). Each covariate (Table 1) was calculated for the contributing area for each of 1,600 reaches in the network.

All models were fitted using a two-step process to (1) describe the spatial autocorrelation structure of $\delta^{18}O$ and (2) to identify covariates that explain the variability in the network mean $\delta^{18}O$. In the first step, models with varying autocorrelation structures were fitted to identify the best structure of $\delta^{18}O$ including all covariates and allowing the slope and intercept for each covariate to vary by each tributary (estimation) or assuming a single slope and intercept per covariate for all tributaries (prediction). The spatial structure uses a moving average construction for autocorrelation based on the shortest distance along the stream network, allowing the spatial autocorrelation to propagate using spatial weights (upstream drainage area). We tested *tail-up* (TU), Euclidean (EU), and both TU and EU distance models (ver Hoef & Peterson, 2010). The TU places more weight on samples upstream and therefore emphasizes the impact of upstream water inputs. The EU method is unbiased with respect to flow direction and consequently emphasizes geographically local inputs. In the second step, models were fitted to predict the mean $\delta^{18}O$ with varying combinations of

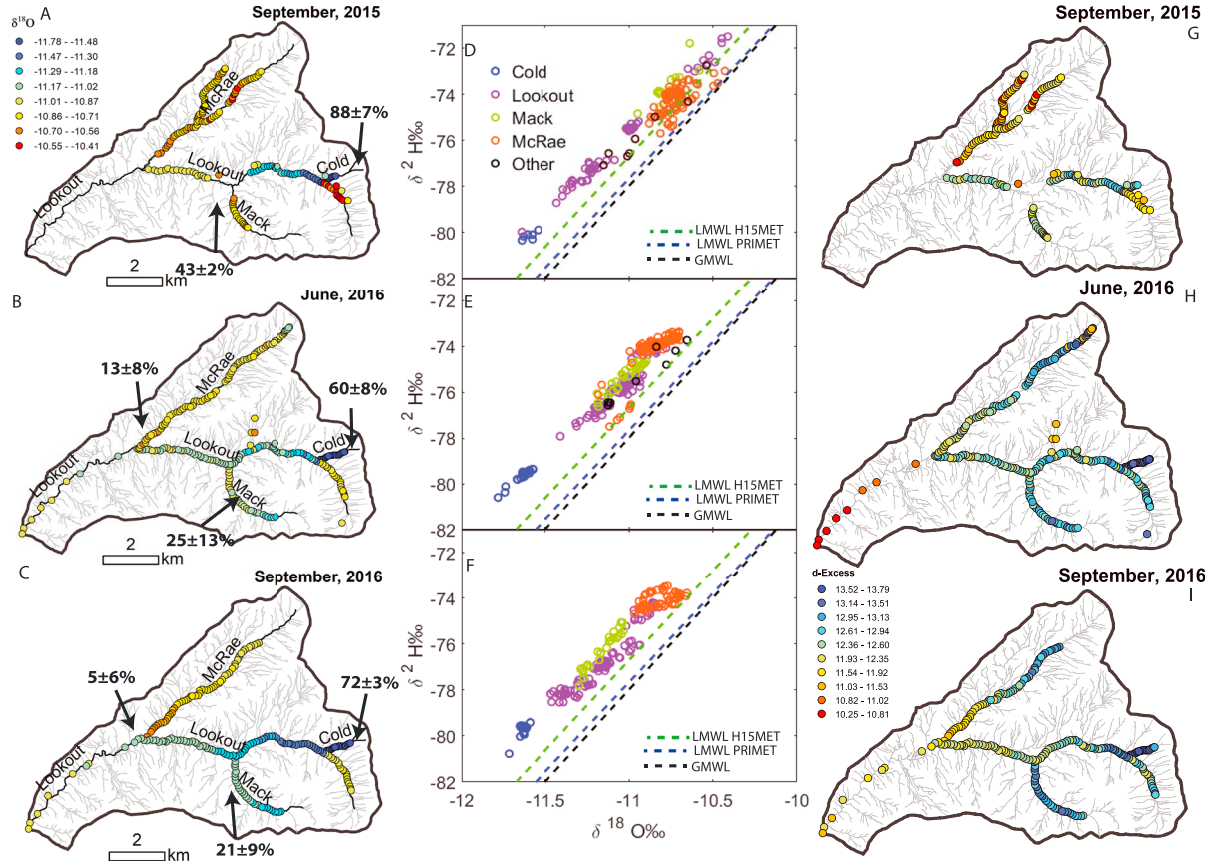

Figure 3. (a–c) $\delta^{18}O$, (d–f) $\delta^{18}O$ and $\delta^{2}H$, and (g–i) deuterium excess in grab samples collected during three synoptic sampling campaigns in September 2015 (a, d, and g) June 2016 (b, e, and h), and September 2016 (c, f, and i). The percentage in Figures 3a–3c indicates the water contributions from Cold, Mack, and McRae Creeks to Lookout Creek at their confluences calculated with the two end-member-mixing model (equations (2) and (3)).

covariates (Table 1), using the best fit autocorrelation structure from step 1. All models in steps 1 and 2 were fitted using maximum likelihood. Best fit models were selected based on the lowest value of the Akaike's Information Criterion (AIC) supplemented by AIC weights (Burnham & Anderson, 2002). Final estimates of parameters in the best-supported models were obtained using restricted maximum likelihood.

3. Results

3.1. Precipitation Isotopic Composition

Between November 2014 and November 2016, values of (precipitation-weighted) $\overline{\delta^{18}O_p}$ and $\overline{\delta^{2}H_p}$ were higher at PRIMET (the low-elevation weather station) than at H15MET (the high-elevation weather station, Figure 2d). At both locations, the mean $\overline{\delta^{18}O_p}$ and $\overline{\delta^{2}H_p}$ averaged over the 12 months prior to sampling were significantly higher for 2015 sampling than for 2016 (Figure 2d). The distinctly drier and warmer conditions experienced in the 2014–2015 period resulted in less precipitation and a more enriched signal (i.e., higher ^{18}O and ^{2}H). The isotopic composition of the precipitation in 2016 was similar to the means reported for the Andrews Forest for 2001 to 2003 (McGuire et al., 2005) and 2006 (Brooks et al., 2010). Precipitation d-excess between November 2014 and November 2016 ranged from 5‰ to 20.8‰. The (precipitation weighted) $\overline{\text{d-excess}}$ over this period was lower at PRIMET (10.75 ± 0.05‰) than at H15MET (11.39 ± 0.08‰, *t* test, $p = 0.00001$).

3.2. Variability in Summer Surface Water Isotopic Composition

The isotopic signature of baseflow varied in space and time (Figure 3). Overall, surface water $\delta^{18}O$ varied from −11.78‰ to −10.4‰ and $\delta^{2}H$ from −80.6‰ to −71.49‰ (Figure 3). Streamflow $\delta^{18}O$ and $\delta^{2}H$ values

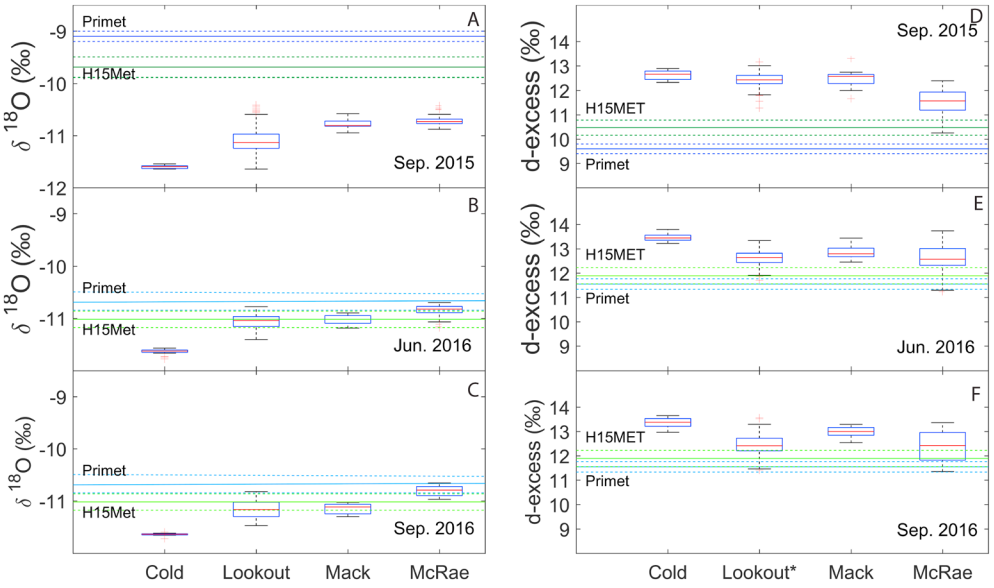

Figure 4. Distributions (boxplots) of $\delta^{18}O$ (a–c) and deuterium excess (d–f) by tributary in September 2015, June 2016, and September 2016 illustrate differences among tributaries and significantly more depleted (lower) $\delta^{18}O$ in all grab samples collected in September 2015 compare to the mean volume-weighted $\delta^{18}O$ and d-excess for the precipitation at PRIMET and H15MET (solid blue and green lines). The 95% confidence interval bounds for the mean precipitation (dashed blue and green lines) are indicated. In 2016 (June and September) the $\delta^{18}O$ of all grab samples except those in Cold Creek all well bounded by the observed $\delta^{18}O$ in the precipitation.

were higher in 2015 (Figure 3d) than in June 2016 (Figure 3e) or September 2016 (Figure 3f). The isotopic composition of streamflow also varied in space. Cold Creek had consistently lower $\delta^{18}O$ and $\delta^{2}H$ values compared to other high-elevation sites in Lookout and McRae Creeks (Figures 3d–3f and 4).

Baseflow amount was not related to drainage area. The two-end member-mixing model indicated that Cold Creek contributed 60.3–72% of the Lookout Creek baseflow during average conditions (June and September 2016, Figures 3b and 3c) and 88% of the baseflow during the drought (2015, Figure 3a). In other words, Cold Creek (91.3 ha) delivered 15 times more water per unit area during baseflow than the remainder of Lookout Creek above the confluence with Cold Creek (539.6 ha). In contrast, baseflow contributions from Mack Creek were roughly proportional to drainage area (Mack Creek is 33% of the drainage area of Lookout Creek at their confluence and contributed 21–25% of baseflow during average conditions and 43% of baseflow during the drought, Figures 3a–3c), whereas baseflow contributions from McRae Creek were relatively low (McRae Creek is 45% of the drainage area of Lookout Creek at their confluence and contributed only 5–13%) during average baseflow (Figures 3b and 3c).

Values of $\delta^{18}O$, $\delta^{2}H$, and d-excess from stream samples indicate temporal and spatial differences in the relative importance of contributions to baseflow from recent precipitation versus water stored in the subsurface. During average conditions (June 2016 and September 2016), the average isotopic composition of baseflow was close to the annual $\overline{\delta^{18}O_p}$ values for all tributaries, except for Cold Creek (Figures 4b and 4c). However, baseflow in all tributaries was more depleted than the annual $\overline{\delta^{18}O_p}$ in 2015 (Figure 4a). The d-excess values for baseflow in 2016 were consistent with the annual $\overline{\text{d-excess}}$ of precipitation in McRae and Lookout Creeks (Figures 4e and 4f). In 2015, however, d-excess values for baseflow were higher than the annual $\overline{\text{d-excess}}$ of precipitation in all tributaries (Figure 4d). This result suggests that a large portion of baseflow in 2015 was derived from stored water rather than recent precipitation.

Spatial patterns of $\delta^{18}O$ and d-excess in baseflow capture differences in contributions of recent precipitation to baseflow (Figures 3 and 4). Values of $\delta^{18}O$ decreased significantly with elevation at Cold, Mack, McRae, and Lookout (including samples below Cold) Creeks during average conditions (June 2016 and September 2016; Figures 5c and 5e, and Table S1 in the supporting information). In contrast, the relationships

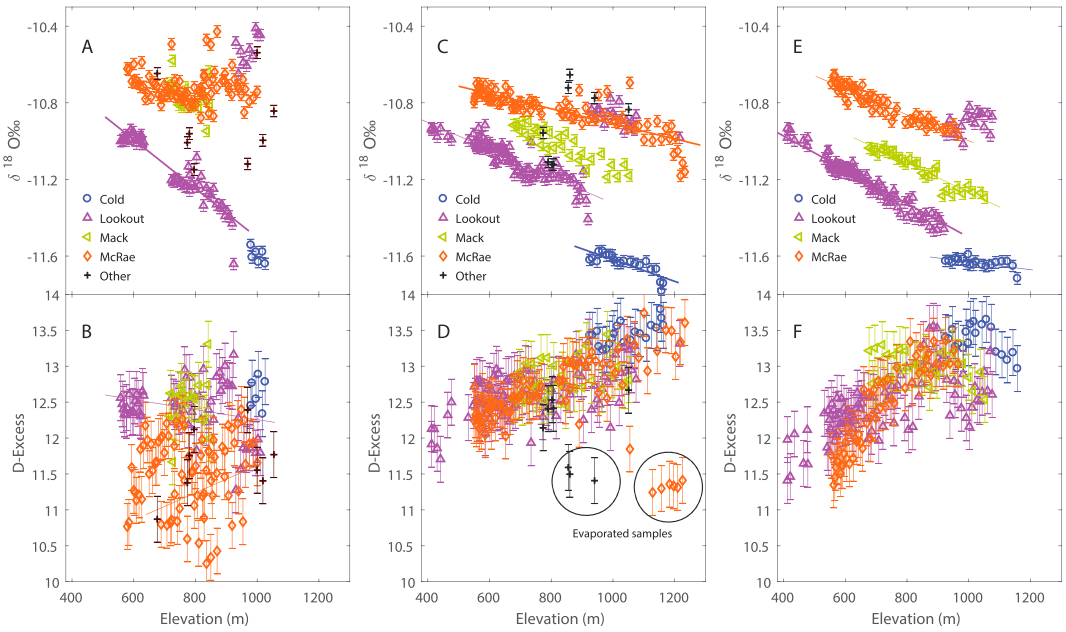

Figure 5. Relationship between elevation and $\delta^{18}O$ and deuterium excess (d-excess) by tributary and sampling campaign. (a and b) September 2015, (c and d) June 2016, and (e and f) September 2016. Error bars represent internal precision based on comparison between duplicates. The samples circled in Figure 5d correspond to evaporated samples. Note the weak correlations with $\delta^{18}O$ for McRae and Mack Creeks in 2015 and for all tributaries with d-excess that year. In contrast, there are strong relationships with $\delta^{18}O$ and d-excess in 2016. Significant regression lines for $\delta^{18}O$ lapse rates by tributary are included (see Table S1 for all lapse rate statistics). The samples in Lookout Creek upstream from the confluence with Cold Creek were excluded for the regression line calculation of Lookout Creek. Figure 5d includes six samples collected in the headwaters of McRae Creek and in three small tributaries to Lookout Creek that given their low d-excess appear to be influenced by evaporation.

between $\delta^{18}O$ and elevation were weak for all tributaries during the drought (2015), except for Lookout Creek (including samples below Cold Creek, Figure 5a). The variation of $\delta^{2}H$ with elevation is similar to that observed for $\delta^{18}O$ (Table S1). The mean $\delta^{18}O$ for Mack Creek, McRae Creek, and Lookout Creek above Cold Creek was close to the regional lapse rate of stream water in the Willamette River basin (Brooks et al., 2012), but the mean $\delta^{18}O$ for Cold Creek and Lookout Creek downstream of Cold Creek plots below the regional lapse rate (Figure 6).

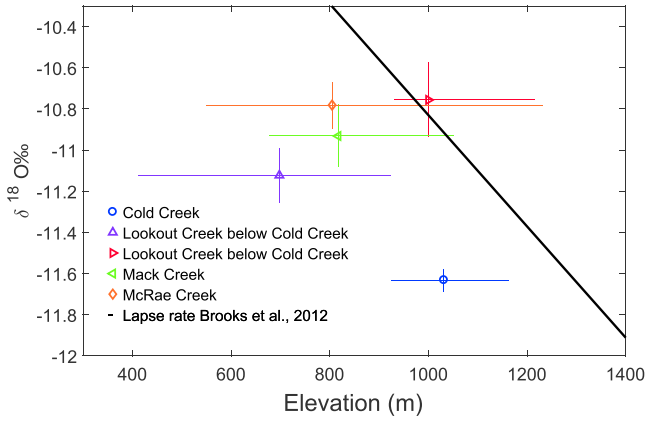

Figure 6. Comparison between the mean $\delta^{18}O$ per tributary and the regional stream isotopic lapse rate for the Willamette River basin (Brooks et al., 2012). Cold Creek and Lookout Creek below the confluence with Cold Creek plot to the left of the lapse rate, indicating a water source higher in elevation than the sampling locations. The horizontal lines depict the range of elevations sampled in each tributary across all samplings, and vertical lines indicate the mean $\delta^{18}O$ ±1 standard deviation.

Mean d-excess values in 2015 at McRae Creek were lower, whereas those in Cold Creek were higher, than in other tributaries in both years (Figures 4d–4f). Values of d-excess increased significantly with elevation for most tributaries in both June and September 2016 (Figures 3h and 3i and 5d and 5f), but d-excess was unrelated to elevation in 2015 (Figure 5b). At McRae Creek, mean d-excess values were significantly lower in 2015 (11.5‰, Figure 4d) than in June or September 2016 (> 12.4‰, Figures 4e and 4f).

3.3. SSN Models to Estimate and Predict $\delta^{18}O$

3.3.1. Estimation Models

The best-supported estimation (E) models explained 94 to 99% of the variation in $\delta^{18}O$ (Table 2). Covariates explained 66% to 83% of the variation, and the autocovariance structure explained 9.1% to 19% (Tables 2 and 3). In all models ($n = 16$) for all sampling periods the *tail-up* autocorrelation structure was the most appropriate to describe the relationship between $\delta^{18}O$ observations based on separation distance. The prevalence of the

Table 2
Parameter Estimates and Summary Statistics for the Best-Supported Spatial Stream Network (SSN) Model to Predict (P) $\delta^{18}O$ and for the Best-Supported SSN Model to Estimate (E) $\delta^{18}O$ for Each Sampling Campaign

						% of variance[g]		
Model[a]	Covariate[b]	b (SE) [c]	CI 95%[d]	Cvr[2e]	RMSE[f]	Cov.	TU	Euc.
2015	Trib*CO	−10.54 (1.62)	[−13.716, −7.37]	0.94	0.068	76.6	12.9	
E1	Trib*LO	0.373 (1.63)	[−2.822, 3.568]					
	Trib*LU	−1.129 (1.929)	[−4.91, 2.651]					
	Trib*MM	0.311 (1.69)	[−3.001, 3.624]					
	Trib*MR	−0.025 (1.627)	[−3.214, 3.163]					
	H:Trib*CO	−0.0011 (0.0016)	[−0.004, 0.002]					
	H:Trib*LO	−0.0003 (0.0016)	[−0.003, 0.003]					
	H:Trib*LU	0.0023 (0.0019)	[−0.001, 0.006]					
	H:Trib*MM	0.0004 (0.0017)	[−0.003, 0.004]					
	H:Trib*MR	0.0009 (0.0016)	[−0.002, 0.004]					
Jun 2016	Trib*CC	−11.08 (0.07)	[−11.227, −10.942]	0.96	0.046	65.6	19	
E2	Trib*LO	0.318 (0.049)	[0.222, 0.413]					
	Trib*LU	0.777 (0.056)	[0.668, 0.887]					
	Trib*MM	0.461 (0.049)	[0.364, 0.558]					
	Trib*MR	0.666 (0.049)	[0.569, 0.763]					
	H	−0.0005 (0.0001)	[−0.0007, −0.0004]					
Sep 2016	Trib*CO	−11.4 (0.14)	[−11.672, −11.121]	0.99	0.031	83.3	9.1	
E1	Trib*LO	0.818 (0.154)	[0.515, 1.12]					
	Trib*LU	0.051 (0.272)	[−0.482, 0.583]					
	Trib*MM	0.777 (0.163)	[0.458, 1.095]					
	Trib*MR	1.024 (0.155)	[0.72, 1.328]					
	H:Trib*CO	−0.0002 (0.0001)	[−0.0005, 0]					
	H:Trib*LO	−0.0007 (0.0002)	[−0.001, −0.0004]					
	H:Trib*LU	0.0007 (0.0003)	[0.0001, 0.0012]					
	H:Trib*MM	−0.0004 (0.0002)	[−0.0007, −0.0001]					
	H:Trib*MR	−0.0004 (0.0002)	[−0.0007, −0.0001]					
2015, P1	Int.	−10.86 (0.09)	[−11.038, −10.69]	0.85	0.11	0.0	53.75	35.87
Jun 2016, P2	Int.	−10.62 (0.15)	[−10.91, −10.335]	0.91	0.073	2.3	94.5	
	H	−0.0004 (0.0002)	[−0.001, 0]					
Sep 2016, P8	Int.	−10.62 (0.13)	[−10.87, −10.37]	0.97	0.043	5.5	91.4	
	H	−0.0003 (0.0001)	[−0.0006, 0]					
	S	−0.0021 (0.0008)	[−0.004, −0.001]					

Note. RMSE = root-mean-square error.
[a]The numbers correspond to those in Table 3. [b]Covariates: Int: intercept; *S*: slope; *H*: elevation; *R*: roughness; and tmt: Area underlain ash-flow tuff. Trib*: indicates that the model considered variations in terms of the mean value (intercept) by tributary (CO: Cold Creek, LO: Lookout below Cold Creek; LU: Lookout above Cold Creek; MM: Mack Creek; and MR: McRae). H:Trib* indicates that the model considered slope variations by tributary. [c]Coefficient value and standard error in parenthesis. [d]95% Confidence intervals. [e]Square correlation between the leave-one-out cross-validation prediction and observed $\delta^{18}O$. [f]Root-mean-square prediction error. [g]Variance explain by covariates and best-supported autocovariance structure (TU, tail-up; Euc, Euclidean; ver Hoef et al., 2014).

tail-up autocorrelation structure is consistent with the predominantly exponential form of the empirical variograms for sampling dates in 2016 (data not shown), which indicates that the $\delta^{18}O$ at a given location depends on $\delta^{18}O$ upstream values at multiple lag distances. Elevation was a covariate in the best-supported estimation models for all sampling campaigns (Tables 2 and 3). During average conditions in June 2016, elevation was the only covariate: $\delta^{18}O$ was negatively related to elevation in the best-supported models that permitted intercepts to vary by tributary, as well as those that permitted intercepts and slopes to vary by tributary (E1 and E2, Tables 2 and 3). In contrast, during drier conditions (2015 and September 2016), the second best-supported model (E12) included elevation and roughness as covariates (Table 3). In the best-supported model for September 2016, $\delta^{18}O$ was negatively related to elevation for all tributaries, except for Lookout Creek upstream from Cold Creek, whereas in the best-supported model for 2015, $\delta^{18}O$ was negatively related to elevation only in Cold Creek and in Lookout Creek below Cold Creek (Figure 5).

3.3.2. Prediction Models

The best-supported prediction (P) models explained 85 to 97% of variation in $\delta^{18}O$; 89 to 94% of the variance in these models was explained primarily by the autocorrelation structures (Table 2). In all models ($n = 13$)

Table 3
Comparison of Spatial Stream Network (SSN) Model Support to Predict (P) and Estimate (E) $\delta^{18}O$ for Each Sampling Campaign Based on the Akaike Information Criteria (AIC), the Change in the AIC Relative to the Best-Supported Model (Δi), and AIC Weights (AIC_w) for the Best Supported (i.e., with $\Delta i < 2$)

		Covariates[a]						September 2015			June 2016			September 2016		
	No.	H	S	R	Lava	tmt	*Np*[b]	AIC	Δi	AIC_w	AIC	Δi	AIC_w	AIC	Δi	AIC_w
E	**1**	**3**					**10**	**−379.9**	**0.0**	**53%**	**−727.4**	**3.5**	**14%**	**−808.8**	**0.0**	**60%**
E	2	2					5				**−730.9**	**0.0**	**83%**			
E	12	3		3			**15**	**−378.4**	**1.6**	**25%**				**−806.7**	**2.2**	**20%**
P	1						1	**−199.0**	**0.0**	**26%**						
P	2	1					2	−197.0	2.0	10%	**−617.3**	**0.0**	**27%**			
P	3				1			−197.1	1.92	10%						
P	4					1	2	−197.1	2.0	10%						
P	5		1				2	**−197.6**	**1.4**	**13%**				**−633.0**	**1.3**	**18%**
P	6			1			2	−197.0	2.0	9%						
P	7	1				1	3				−615.4	1.9	10%			
P	8	1	1				3				−615.9	1.4	13%	**−634.3**	**0.0**	**33%**
P	9	1		1			3				**−616.6**	**0.7**	**19%**			
P	12	1	1			1	4							−632.7	1.5	16%

Note. All relationships between covariates and $\delta^{18}O$ were negative within the prediction models. Top two models in each campaign are in bold.
[a]Covariates included elevation (*H*), percent of contributing area underlain by lava flows (lava) or ash-flow tuff (tmt), slope (*S*), and roughness (*R*); 1: models with the same intercept and slope of the relations between covariates and $\delta^{18}O$, 2: models with varying intercept by tributary, and 3: models with both intercept and slope varying by tributary. [b]Number of model parameters. In addition, SSN models include three to seven parameters associated with the autocovariance construction (ver Hoef & Peterson, 2010). A complete list of all the models considered is included in Table S2.

for sampling periods in 2016 the tail-up autocorrelation structure was identified as the most appropriate (Table 2). However, in models for 2015, Euclidian distance was also part of the best-supported autocorrelation structure. This is consistent with the spherical shapes of the empirical semivariograms for 2015 (data not shown) and indicates that the $\delta^{18}O$ at a given location in 2015 also depends on neighboring values at short lag distances. Because only a small proportion of the variation was explained by the covariates, multiple alternative combinations of covariates were present in the predictive models that were similarly well supported (Table 3).

Catchment wide isoscapes for $\delta^{18}O$ created from the best-supported predictive models (Figure 7) highlight the distinct patterns of baseflow isotopic composition during the drought period (September 2015) compared to average flow conditions (June 2016). The values of $\delta^{18}O$ were significantly higher (more enriched) in most of the stream network in 2015 compared to 2016. In 2015, patches of relatively depleted baseflow are evident near deep-seated earthflows (Figures 1 and 7). Baseflow was also consistently depleted for both years in Cold Creek and Lookout Creek downstream from Cold Creek. The standard error in the predictions increases away from the sampling points (Figure S1).

Allowing the mean of $\delta^{18}O$ (intercept) to change from tributary to tributary increased the amount of variation explained by the estimation models compared to the predictive models (Table 2). Nevertheless, similar covariates were included in the best-supported estimation and predictive models for each sampling period (Table 3) with similar predictions and estimations at the sampling locations (Figure S2).

4. Discussion

4.1. Conceptual Model of Baseflow Water Sources

These findings suggest a conceptual model of baseflow sources in response to climate variability (Figure 8). During years with average snowpack and average baseflow conditions, baseflow isotopic composition is strongly related to elevation, reflecting the influence of stored water derived from snowmelt (Figure 8a). In contrast, during years with low snowpack and severe summer drought conditions, baseflow isotopic analysis suggests that more of the baseflow water originated from stored water derived from geomorphic features (e.g., deep-seated earthflows) rather than from recent precipitation (Figure 8b). Water storage in high-elevation geologic features (i.e., porous lava flows) also influences baseflow isotopic composition (Figure 8c).

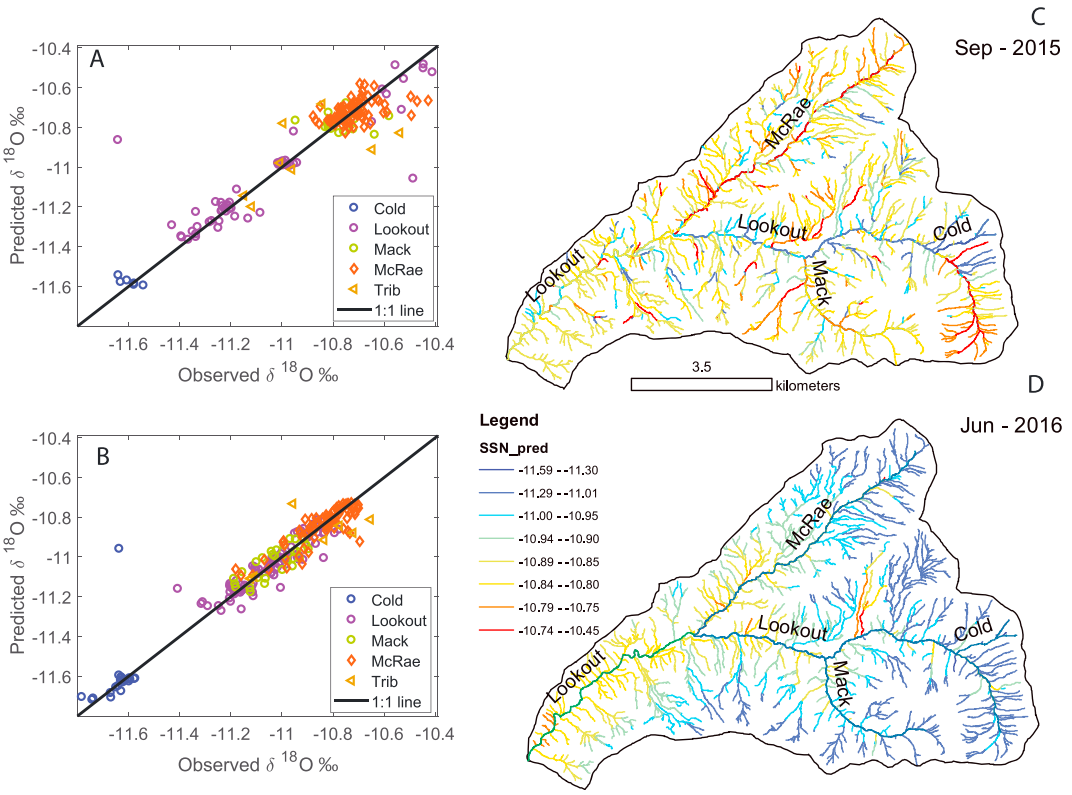

Figure 7. (a and b) Spatial Stream Network (SSN) models for September 2015 and June 2016. Black lines indicate 1:1 relationship. (c and d) Isoscape maps of $\delta^{18}O$ predicted by the SSN model fit to samples collected in 2015 and June 2016. Streamlines are colored by the predicted values. The model used in Figure 7c was P1, and the model used in Figure 7d was P2 (Table 2).

In years with average precipitation and snowpack, elevation influences precipitation, snowpack, and, thereby, baseflow isotopic composition (Figure 8a). In 2016, snowpack water equivalent approached 1,000 mm, precipitation and stream water isotopic composition were similar, d-excess was positively related to elevation, and elevation was a covariate in best-supported geostatistical models of baseflow isotopic composition. Baseflow isotopic signature is correlated with elevation because isotopic composition becomes progressively depleted of heavy isotopes (^{18}O and ^{2}H) with increasing elevation (Araguas-Araguas et al., 2000; Fan et al., 2015; Peng et al., 2015; Vespasiano et al., 2015; Wassenaar et al., 2011). Values of d-excess are frequently positively correlated to elevation in mountainous regions (Bershaw et al., 2012; Gonfiantini et al., 2001; Liotta et al., 2013). For example, winter precipitation in Canadian mountain sites with Pacific Ocean water sources, similar to the study site, has particularly high d-excess values (Froehlich et al., 2002).

In contrast, in years with low snowpack, geomorphic features such as deep earthflows influence the isotopic signature of baseflow (Figure 8b). In 2015, snowpack water equivalent did not exceed 200 mm, precipitation and stream water isotopic composition were different, d-excess was not related to elevation, and slope and surface roughness were covariates in best-supported geostatistical models of baseflow isotopic composition. The lack of correlation in 2015 between elevation and $\delta^{18}O$ and $\delta^{2}H$ observed in all tributaries except Lookout Creek below Cold Creek indicates that the strength of these relationships is a function of precipitation amount and corroborates that precipitation amount and composition in 2015 were not important factors for summer baseflow isotopic values. Deviations from the expected expression of the rainout effect (i.e., decreasing $\delta^{18}O$ and $\delta^{2}H$ with elevation) in stream water have been reported in other catchments and attributed to the effects of atmospheric recycling and complex vapor sources (Bershaw et al., 2012; Lechler & Niemi, 2011), the effects of lower precipitation amount in catchments located within topographic rain shadows (Brooks et al., 2012), or interbasin water contributions (Nickolas et al., 2017). The lack of correlation of d-excess with elevation in 2015 may be associated with competition between controls on d-excess, including

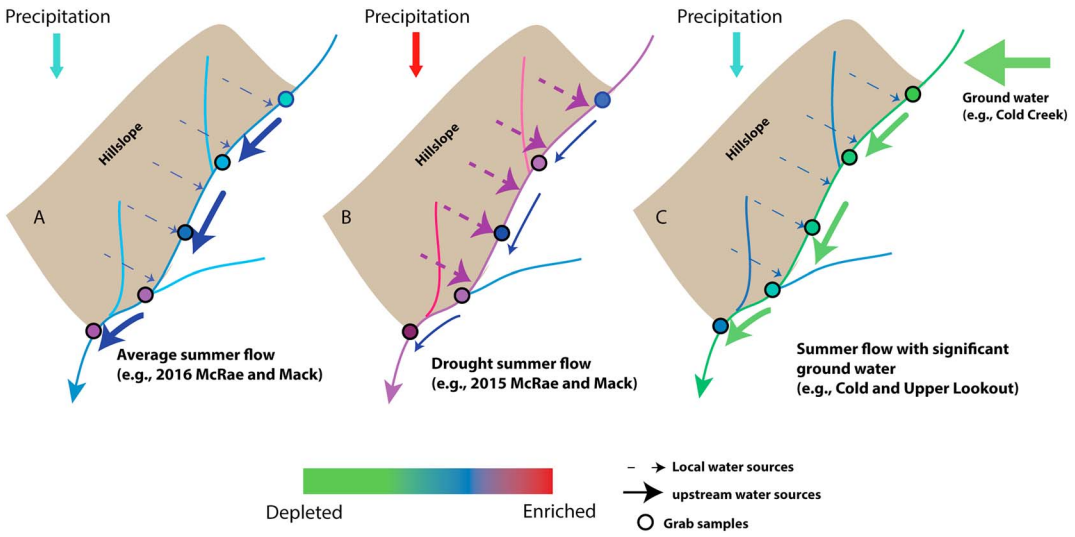

Figure 8. Conceptual diagram of water sources during average and drought conditions. Line thickness of the arrows represents the relative contribution of the source, and the tint (from red to green) represents the value of $\delta^{18}O$. Figure 8a represents a situation in which the effects of elevation on the precipitation amount and type are strong and thus streams dependent on local water sources. Figure 8b represents the effects of subsurface storage, that is, deep-seated earthflows (as indicated by low slope) on baseflow, and Figure 8c represents a stream in which the effects of subsurface storage, that is, lava flows (as indicated by geologic substrate) are strong and thus the sources of water appear to be independent of recent local precipitation producing the same patterns during average and drought conditions. The precipitation in drought conditions (Figure 8b) is indicated as relatively more enriched than during average conditions because small fractionation rates are expected during a warm drought.

evaporation of some fraction of rainfall as it fell, local moisture recycling (Camille et al., 2013), local evaporation, or the lack of the major snowmelt flux into streams (Merlivat & Jouzel, 1979), all of which were likely enhanced by the high mean temperature and relatively low precipitation of 2015 compared to the average year (2016).

The interpretations about differences in water sources between average and drought conditions were very clear in our case given that $\delta^{18}O$ and $\delta^{2}H$ were higher in 2015 precipitation compared to 2016 precipitation. Precipitation was more enriched in 2015 because of smaller fractionation rates due to the higher temperatures in this year, consistent with model simulations (Liu et al., 2014; Nusbaumer et al., 2017; Nusbaumer & Noone, 2018). This strong contrast in precipitation isotopes between years enhanced our ability to demonstrate that summer baseflow during the drought did not originate from the recent precipitation.

Geomorphic features such as earthflows may provide a source of baseflow in years with little snowpack and very low summer streamflow (Figure 8b). The importance of geomorphic features such as deep-seated earthflows as baseflow sources is supported by the depleted isotopic composition of baseflow relative to precipitation in the drought year (2015), the lack of correlation between d-excess, $\delta^{18}O$, or $\delta^{2}H$ and elevation in most tributaries in 2015, and the inclusion of slope and roughness as covariates in best-supported SSN models for the drought year. Deep-seated earthflows mapped in the study area (Swanson & James, 1975) coincide with areas of relatively low spatial variation in isotopic values in 2015 (Figures 1 and 3a). These findings imply that baseflow in 2015 was sourced from connected water stored within these deep-seated earthflows (Swanson & James, 1975). However, samples from this water (or tracer tests) would be needed to fully confirm this interpretation. Earthflows are characterized by relatively low slope and high surface roughness. Surface roughness can indicate soil thickness (Patton et al., 2018), which in turn is linked to shallow groundwater (Schulz et al., 2008), baseflow variability during drought conditions (Price et al., 2011), and groundwater supply (Tetzlaff & Soulsby, 2008). Other studies also demonstrate that hillslope characteristics (e.g., slope and roughness) influence baseflow (Jencso & McGlynn, 2011; McGuire et al., 2005; Singh et al., 2016; Zimmer & Gannon, 2018), particularly during dry conditions (Heidbuchel et al., 2013).

Geologic features, such as porous lava flows, also influence baseflow isotopic composition (Figure 8c). The ridge-capping materials are located on southern and eastern upper slopes (Figure 1) and are a mixture of aa lava flows, rounded gravels, and ash deposits (Swanson & Jones, 2002; Walker & MacLeod, 1991). The significantly depleted baseflow isotopic signatures and relatively high unit-area baseflow contributions at Cold Creek in both 2015 and 2016 imply that baseflow in Cold Creek is derived from stored water in these lava flows. The higher d-excess and more depleted (i.e., lower) $\delta^{18}O$ of Cold Creek compared to the precipitation in both 2015 and 2016 and compared to regional streamflow samples (Figure 6) also imply that baseflow may be sourced from snowmelt that formed at a higher elevation and lower temperature (Bershaw et al., 2012; Gonfiantini et al., 2001; Liotta et al., 2013). The study area is separated by faulting from the regional groundwater of the High Cascades (Ingebritsen et al., 1994), indicating that the groundwater source to Cold Creek is likely local. Other studies have also illustrated that springs emerging from lava flow deposits are an important source of baseflow (Fujimoto et al., 2016; Jefferson et al., 2006).

The SSN estimation models revealed the importance of covariates, such as elevation, slope angle, surface roughness, and geology, which in turn permitted interpretations of processes that contribute to the spatial and temporal patterns of baseflow isotopic conditions. In contrast, the SSN prediction models relied primarily on the autocorrelation structure and covariates were less important. This resulted in decreased model accuracy away from the sampled tributaries particularly in 2015, for which the best prediction model did not include any of the covariates.

4.2. Implications for Future Drought Conditions

Climate change in the Pacific Northwest is reducing snowpacks (Mote et al., 2016). This study showed that when a snowpack was present, sources of stored water to baseflow were concentrated at high elevation, but when snowpack was absent, sources of stored water to baseflow shifted to areas with porous lava flows or areas with lower slope angles and higher surface roughness that were mapped as deep-seated earthflows. Thus, when there is little or no snowpack, spring-fed systems become more important to summer baseflow. Groundwater-fed streams are relatively resilient to drought (Zimmer & Gannon, 2018), and regional groundwater systems in the High Cascades (east of the study area) might mediate streamflow in the face of greater climate variability (Mayer & Naman, 2011; Safeeq et al., 2014; Tague & Grant, 2009). Deep earthflows and associated deep flow path groundwater sources will become increasingly important to mediate drought impacts on stream networks as snowpacks decline under future climate conditions. Understanding the different sources and residence times of water contributing to baseflow will therefore be critical for effective water resource management under future climate conditions in mountain catchments worldwide.

5. Conclusions

Although surface topography, geology, and geomorphic features all influence contributions to summer baseflow, the importance of these factors differs with climate. Spatial patterns of precipitation strongly influence the contributions to baseflow during an average water year, but geomorphic features, especially deep earthflows, emerged as important controls on contributions to baseflow in a drought year with little or no snowpack. Geologic features, especially porous substrate, explained the contributions to baseflow as well as spatial patterns of unit-area discharge in both average and drought conditions. Spatially explicit models of the $\delta^{18}O$ isoscape illustrated how baseflow patterns may shift under conditions of very low snowpack, which may be more frequent in the future. Under projected warming conditions with declining snowpack, baseflow discharge in midsized stream catchments will become increasingly reliant on the disproportionate contribution from subcatchments with groundwater sources. In mountain landscapes with variable geologic and geomorphic features the sources of baseflow that sustain stream ecosystems vary greatly depending not only on recent precipitation contributions but also on the presences of Quaternary deposits and porous volcanic bedrock.

Acknowledgments
We would like to thank Sam Swanson and Stanley French for collecting many of the baseflow samples and to Greg Downing and Greg Cohn who collected the precipitation samples. Spatial and hydrometric data were provided by the HJ Andrews Experimental Forest and Long Term Ecological Research program, administered cooperatively by the USDA Forest Service Pacific Northwest Research Station, Oregon State University, and the Willamette National Forest. This material is based upon work supported by the National Science Foundation under Grant DEB-1440409. These data and the isotopic data collected are freely available from the H. J. Andrews Experimental Forest research program (http://andrewsforest.oregonstate.edu/). This research was funded in part by the National Science Foundation under grants DEB-1440409, AGS-0955841, and DEB 1547628, and by the USDA National Institute of Food and Agriculture (McIntire Stennis project OREZ-FERM-876). The College of Forestry at Oregon State University provided funding for J. Tenny through the Undergraduate Mentored Employment Program. Many thanks to Fred Swanson, Steve Wondzell, Anne Jefferson, and Gordon Grant for insightful discussions about the Andrews Forest, and to Erin Peterson, Jay Ver Hoef, and Daniel Isaak for discussions about the application of Spatial Stream Network models.

References

Alexander, R. B., Boyer, E. W., Smith, R. A., Schwarz, G. E., & Moore, R. B. (2007). The role of headwater streams in downstream water quality1. *Journal of the American Water Resources Association*, *43*(1), 41–59. https://doi.org/10.1111/j.1752-1688.2007.00005.x

Araguas-Araguas, L., Froehlich, K., & Rozanski, K. (2000). Deuterium and oxygen-18 isotope composition of precipitation and atmospheric moisture. *Hydrological Processes*, *14*(8), 1341–1355. https://doi.org/10.1002/1099-1085(20000615)14:8<1341::AID-HYP983>3.3.CO;2-Q

Bershaw, J., Penny, S. M., & Garzione, C. N. (2012). Stable isotopes of modern water across the Himalaya and eastern Tibetan Plateau: Implications for estimates of paleoelevation and paleoclimate. *Journal of Geophysical Research*, *117*, D02110. https://doi.org/10.1029/2011JD016132

Beven, K. J., & Kirkby, M. J. (1979). A physically based, variable contributing area model of basin hydrology. *Hydrological Sciences Bulletin*, *24*(1), 43–69. https://doi.org/10.1080/02626667909491834

Bloomfield, J. P., Allen, D. J., & Griffiths, K. J. (2009). Examining geological controls on baseflow index (BFI) using regression analysis: An illustration from the Thames basin, UK. *Journal of Hydrology*, *373*(1-2), 164–176. https://doi.org/10.1016/j.jhydrol.2009.04.025

Blumstock, M., Tetzlaff, D., Malcolm, I. A., Nuetzmann, G., & Soulsby, C. (2015). Baseflow dynamics: Multi-tracer surveys to assess variable groundwater contributions to montane streams under low flows. *Journal of Hydrology*, *527*, 1021–1033. https://doi.org/10.1016/j.jhydrol.2015.05.019

Bowen, G. J. (2010). Isoscapes: Spatial pattern in isotopic biogeochemistry. *Annual Review of Earth and Planetary Sciences*, *38*, 161–187.

Bowen, G. J., Ehleringer, J. R., Chesson, L. A., Stange, E., & Cerling, T. E. (2007). Stable isotope ratios of tap water in the contiguous United States. *Water Resources Research*, *43*, W03419. https://doi.org/10.1029/2006WR005186

Brennan, S. R., Torgersen, C. E., Hollenbeck, J. P., Fernandez, D. P., Jensen, C. K., & Schindler, D. E. (2016). Dendritic network models: Improving isoscapes and quantifying influence of landscape and in-stream processes on strontium isotopes in rivers. *Geophysical Research Letters*, *43*, 5043–5051. https://doi.org/10.1002/2016GL068904

Brooks, J. R., Barnard, H. R., Coulombe, R., & McDonnell, J. J. (2010). Ecohydrologic separation of water between trees and streams in a Mediterranean climate. *Nature Geoscience*, *3*(2), 100–104. https://doi.org/10.1038/NGEO722

Brooks, J. R., Wigington, P. J., Phillips, D. L., Comeleo, R., & Coulombe, R. (2012). Willamette River basin surface water isoscape (delta O-18 and delta H-2): Temporal changes of source water within the river. *Ecosphere*, *3*(5), art39. https://doi.org/10.1890/es11-00338.1

Burnham, K. P., & Anderson, D. R. (2002). *Model Selection and Multimodel Inference*. New York.: Springer.

Camille, R., David, N., Christian, F., & John, W. (2013). Role of continental recycling in intraseasonal variations of continental moisture as deduced from model simulations and water vapor isotopic measurements. *Water Resources Research*, *49*, 4136–4156. https://doi.org/10.1002/wrcr.20312

Cavalli, M., Tarolli, P., Marchi, L., & Dalla Fontana, G. (2008). The effectiveness of airborne LiDAR data in the recognition of channel-bed morphology. *Catena*, *73*(3), 249–260. https://doi.org/10.1016/j.catena.2007.11.001

Craig, H. (1961). Isotopic variations in meteoric waters. *Science*, *133*(3465), 1702–1703. https://doi.org/10.1126/science.133.3465.1702

Daly, C., & McKee, W. A. (2016). Meteorological data from benchmark stations at the Andrews Experimental Forest, 1957 to present. Long-Term Ecological Research. Forest Science Data Bank, Corvallis, OR. [Database]. Available: http://andlter.forestry.oregonstate.edu/data/abstract.aspx?dbcode=MS001 (4 November 2018). https://doi.org/10.6073/pasta/c96875918bb9c86d330a457bf4295cd9

Dutton, A., Wilkinson, B. H., Welker, J. M., Bowen, G. J., & Lohmann, K. C. (2005). Spatial distribution and seasonal variation in 18O/16O of modern precipitation and river water across the conterminous USA. *Hydrological Processes*, *19*(20), 4121–4146. https://doi.org/10.1002/hyp.5876

Fan, Y., Chen, Y., Li, X., Li, W., & Li, Q. (2015). Characteristics of water isotopes and ice-snowmelt quantification in the Tizinafu River, north Kunlun Mountains, Central Asia. *Quaternary International*, *380–381*, 116–122. https://doi.org/10.1016/j.quaint.2014.05.020

Farvolden, R. N. (1963). Geologic controls on ground-water storage and base flow. *Journal of Hydrology*, *1*(3), 219–249. https://doi.org/10.1016/0022-1694(63)90004-0

Fischer, B. M. C., Rinderer, M., Schneider, P., Ewen, T., & Seibert, J. (2015). Contributing sources to baseflow in pre-alpine headwaters using spatial snapshot sampling. *Hydrological Processes*, *29*(26), 5321–5336. https://doi.org/10.1002/hyp.10529

Freeman, M. C., Pringle, C. M., & Jackson, C. R. (2007). Hydrologic connectivity and the contribution of stream headwaters to ecological integrity at regional scales 1. *Journal of the American Water Resources Association*, *43*(1), 5–14. https://doi.org/10.1111/j.1752-1688.2007.00002.x

Froehlich, K., Gibson, J. J., & Aggarwal, P. K. (2002). Deuterium excess in precipitation and its climatological significance. Retrieved from International Atomic Energy Agency (IAEA).

Fujimoto, M., Ohte, N., Kawasaki, M., Osaka, K., Itoh, M., Ohtsuka, I., & Itoh, M. (2016). Influence of bedrock groundwater on streamflow characteristics in a volcanic catchment. *Hydrological Processes*, *30*(4), 558–572. https://doi.org/10.1002/hyp.10558

Genereux, D. (1998). Quantifying uncertainty in tracer-based hydrograph separations. *Water Resources Research*, *34*(4), 915–919. https://doi.org/10.1029/98WR00010

Gonfiantini, R., Roche, M.-A., Olivry, J.-C., Fontes, J.-C., & Zuppi, G. M. (2001). The altitude effect on the isotopic composition of tropical rains. *Chemical Geology*, *181*(1-4), 147–167. https://doi.org/10.1016/S0009-2541(01)00279-0

Groning, M., Lutz, H. O., Roller-Lutz, Z., Kralik, M., Gourcy, L., & Poltenstein, L. (2012). A simple rain collector preventing water re-evaporation dedicated for delta O-18 and delta H-2 analysis of cumulative precipitation samples. *Journal of Hydrology*, *448-449*, 195–200. https://doi.org/10.1016/j.jhydrol.2012.04.041

Hale, V. C., & McDonnell, J. J. (2016). Effect of bedrock permeability on stream base flow mean transit time scaling relations: 1. A multiscale catchment intercomparison. *Water Resources Research*, *52*, 1358–1374. https://doi.org/10.1002/2014wr016124

Heidbuchel, I., Troch, P. A., & Lyon, S. W. (2013). Separating physical and meteorological controls of variable transit times in zero-order catchments. *Water Resources Research*, *49*, 7644–7657. https://doi.org/10.1002/2012wr013149

Ingebritsen, S. E., Mariner, R. H., & Sherrod, D. R. (1994). Hydrothermal systems of the Cascade Range, north-central Oregon (1044 L). Retrieved from http://pubs.er.usgs.gov/publication/pp1044L

Isaak, D. J., Hoef, J. M. V., Peterson, E. E., Horan, D. L., & Nagel, D. E. (2017). Scalable population estimates using spatial-stream-network (SSN) models, fish density surveys, and national geospatial database frameworks for streams. *Canadian Journal of Fisheries and Aquatic Sciences*, *74*(2), 147–156. https://doi.org/10.1139/cjfas-2016-0247

Isaak, D. J., Luce, C. H., Rieman, B. E., Nagel, D. E., Peterson, E. E., Horan, D. L., et al. (2010). Effects of climate change and wildfire on stream temperatures and salmonid thermal habitat in a mountain river network. *Ecological Applications*, *20*(5), 1350–1371. https://doi.org/10.1890/09-0822.1

Isaak, D. J., Peterson, E. E., Ver Hoef, J. M., Wenger, S. J., Falke, J. A., Torgersen, C. E., et al. (2014). Applications of spatial statistical network models to stream data. *Wiley Interdisciplinary Reviews Water*, *1*(3), 277–294. https://doi.org/10.1002/wat2.1023

Jefferson, A., Grant, G., & Rose, T. (2006). Influence of volcanic history on groundwater patterns on the west slope of the Oregon High Cascades. *Water Resources Research*, *42*, W12411. https://doi.org/10.1029/2005WR004812

Jencso, K. G., & McGlynn, B. L. (2011). Hierarchical controls on runoff generation: Topographically driven hydrologic connectivity, geology, and vegetation. *Water Resources Research*, *47*, W11527. https://doi.org/10.1029/2011WR010666

Jennings, K., & Jones, J. A. (2015). Precipitation-snowmelt timing and snowmelt augmentation of large peak flow events, western Cascades, Oregon. *Water Resources Research*, *51*, 7649–7661. https://doi.org/10.1002/2014wr016877

Johnson, S., & Lienkaemper, G. (2016). Stream network from 1997 survey and 2008 LiDAR flight, Andrews Experimental Forest. Long-Term Ecological Research. Forest Science Data Bank, Corvallis, OR. [Database]. Available: http://andlter.forestry.oregonstate.edu/data/abstract.aspx?dbcode=HF013 (27 September 2018). https://doi.org/10.6073/pasta/66d98881d4eb6bb5dedcbdb60dbebafa

Jones, J. A., & Perkins, R. M. (2010). Extreme flood sensitivity to snow and forest harvest, western Cascades, Oregon, United States. *Water Resources Research*, *46*, W12512. https://doi.org/10.1029/2009WR008632

Kaylor, M. J., VerWey, B. J., Cortes, A., & Warren, D. R. (2019). Drought impacts to trout and salamanders in cool, forested headwater ecosystems in the western Cascade Mountains, OR. *Hydrobiologia*, *833*(1), 65–80. https://doi.org/10.1007/s10750-019-3882-2

Kendall, C., & Coplen, T. B. (2001). Distribution of oxygen-18 and deuterium in river waters across the United States. *Hydrological Processes*, *15*(7), 1363–1393. https://doi.org/10.1002/hyp.217

Lechler, A. R., & Niemi, N. A. (2011). Controls on the spatial variability of modern meteoric delta o-18: Empirical constraints from the Western US and East Asia and implications for stable isotope studies. *American Journal of Science*, *311*(8), 664–700. https://doi.org/10.2475/08.2011.02

Liotta, M., Grassa, F., D'Alessandro, W., Favara, R., Gagliano Candela, E., Pisciotta, A., & Scaletta, C. (2013). Isotopic composition of precipitation and groundwater in Sicily, Italy. *Applied Geochemistry*, *34*, 199–206. https://doi.org/10.1016/j.apgeochem.2013.03.012

Liu, Z., Yoshmura, K., Bowen, G. J., & Welker, J. M. (2014). Pacific–North American teleconnection controls on precipitation isotopes (δ18O) across the contiguous United States and adjacent regions: A GCM-based analysis. *Journal of Climate*, *27*(3), 1046–1061. https://doi.org/10.1175/jcli-d-13-00334.1

Mayer, T. D., & Naman, S. W. (2011). Streamflow response to climate as influenced by geology and elevation. *Journal of the American Water Resources Association*, *47*(4), 724–738. https://doi.org/10.1111/j.1752-1688.2011.00537.x

McGuire, K. J., McDonnell, J. J., Weiler, M., Kendall, C., McGlynn, B. L., Welker, J. M., & Seibert, J. (2005). The role of topography on catchment-scale water residence time. *Water Resources Research*, *41*, W05002. https://doi.org/10.1029/2004WR003657

McKenzie, N. J., & Ryan, P. J. (1999). Spatial prediction of soil properties using environmental correlation. *Geoderma*, *89*(1-2), 67–94. https://doi.org/10.1016/S0016-7061(98)00137-2

Merlivat, L., & Jouzel, J. (1979). Global climatic interpretation of the deuterium-oxygen 18 relationship for precipitation. *Journal of Geophysical Research*, *84*(C8), 5029–5033. https://doi.org/10.1029/JC084iC08p05029

Meyer, J. L., Wallace, J. B., Press, M. C., Huntly, N. J., & Levin, S. (2001). Lost linkages and lotic ecology: Rediscovering small streams. In M. Press, N. Huntly, & S. Levin (Eds.), *Ecology: Achievement and Challenge* (pp. 295–317). Oxford, UK: Blackwell Scientific.

Mote, P. W., Li, S., Lettenmaier, D. P., Xiao, M., & Engel, R. (2018). Dramatic declines in snowpack in the western US. *Npj Climate and Atmospheric Science*, *1*(1), 2. https://doi.org/10.1038/s41612-018-0012-1

Mote, P. W., Rupp, D. E., Li, S., Sharp, D. J., Otto, F., Uhe, P. F., et al. (2016). Perspectives on the causes of exceptionally low 2015 snowpack in the western United States. *Geophysical Research Letters*, *43*, 10,980–10,988. https://doi.org/10.1002/2016GL069965

Mountain, N., James, A. L., & Chutko, K. (2015). Groundwater and surface water influences on streamflow in a mesoscale Precambrian Shield catchment. *Hydrological Processes*, *29*(18), 3941–3953. https://doi.org/10.1002/hyp.10590

Nickolas, L. B., Segura, C., & Brooks, J. R. (2017). The influence of lithology on surface water sources. *Hydrological Processes*, *31*(10), 1913–1925. https://doi.org/10.1002/hyp.11156

Nusbaumer, J., & Noone, D. (2018). Numerical evaluation of the modern and future origins of atmospheric river moisture over the West Coast of the United States. *Journal of Geophysical Research: Atmospheres*, *123*, 6423–6442. https://doi.org/10.1029/2017JD028081

Nusbaumer, J., Wong, T. E., Bardeen, C., & Noone, D. (2017). Evaluating hydrological processes in the Community Atmosphere Model Version 5 (CAM5) using stable isotope ratios of water. *Journal of Advances in Modeling Earth Systems*, *9*, 949–977. https://doi.org/10.1002/2016MS000839

Ogrinc, N., Kanduč, T., Stichler, W., & Vreča, P. (2008). Spatial and seasonal variations in δ18O and δD values in the River Sava in Slovenia. *Journal of Hydrology*, *359*(3–4), 303–312. https://doi.org/10.1016/j.jhydrol.2008.07.010

Patton, N. R., Lohse, K. A., Godsey, S. E., Crosby, B. T., & Seyfried, M. S. (2018). Predicting soil thickness on soil mantled hillslopes. *Nature Communications*, *9*(1), 3329. https://doi.org/10.1038/s41467-018-05743-y

Pelletier, J. D., Broxton, P. D., Hazenberg, P., Zeng, X., Troch, P. A., Niu, G.-Y., et al. (2016). A gridded global data set of soil, intact regolith, and sedimentary deposit thicknesses for regional and global land surface modeling. *Journal of Advances in Modeling Earth Systems*, *8*, 41–65. https://doi.org/10.1002/2015MS000526

Peng, T.-R., Chen, K.-Y., Zhan, W.-J., Lu, W.-C., & Tong, L.-T. J. (2015). Use of stable water isotopes to identify hydrological processes of meteoric water in montane catchments. *Hydrological Processes*, *29*(23), 4957–4967. https://doi.org/10.1002/hyp.10557

Peralta-Tapia, A., Sponseller, R. A., Ågren, A., Tetzlaff, D., Soulsby, C., & Laudon, H. (2015). Scale-dependent groundwater contributions influence patterns of winter baseflow stream chemistry in boreal catchments. *Journal of Geophysical Research: Biogeosciences*, *120*, 847–858. https://doi.org/10.1002/2014JG002878

Peterson, E., & ver Hoef, J. (2014). STARS: An ArcGIS toolset used to calculate the spatial information needed to fit spatial statistical models to stream network data. *Journal of Statistical Software*, *56*(2), 17. https://doi.org/10.18637/jss.v056.i02

Peterson, E. E., & ver Hoef, J. M. (2010). A mixed-model moving-average approach to geostatistical modeling in stream networks. *Ecology*, *91*(3), 644–651. https://doi.org/10.1890/08-1668.1

Pfister, L., Martinez-Carreras, N., Hissler, C., Klaus, J., Carrer, G. E., Stewart, M. K., & McDonnell, J. J. (2017). Bedrock geology controls on catchment storage, mixing, and release: A comparative analysis of 16 nested catchments. *Hydrological Processes*, *31*(10), 1828–1845. https://doi.org/10.1002/hyp.11134

Price, K. (2011). Effects of watershed topography, soils, land use, and climate on baseflow hydrology in humid regions: A review. *Progress in Physical Geography*, *35*(4), 465–492. https://doi.org/10.1177/0309133311402714

Price, K., Jackson, C. R., Parker, A. J., Reitan, T., Dowd, J., & Cyterski, M. (2011). Effects of watershed land use and geomorphology on stream low flows during severe drought conditions in the southern Blue Ridge Mountains, Georgia and North Carolina, United States. *Water Resources Research*, *47*, W02516. https://doi.org/10.1029/2010WR009340

Saar, M. O., & Manga, M. (2004). Depth dependence of permeability in the Oregon Cascades inferred from hydrogeologic, thermal, seismic, and magmatic modeling constraints. *Journal of Geophysical Research*, *109*, B04204. https://doi.org/10.1029/2003JB002855

Safeeq, M., Grant, G. E., Lewis, S. L., Kramer, M. G., & Staab, B. (2014). A hydrogeologic framework for characterizing summer streamflow sensitivity to climate warming in the Pacific Northwest, USA. *Hydrology and Earth System Sciences*, *18*(9), 3693–3710. https://doi.org/10.5194/hess-18-3693-2014

Schulz, W. H., Lidke, D. J., & Godt, J. W. (2008). Modeling the spatial distribution of landslide-prone colluvium and shallow groundwater on hillslopes of Seattle, WA. *Earth Surface Processes and Landforms*, *33*(1), 123–141. https://doi.org/10.1002/esp.1535

Singh, N. K., Emanuel, R. E., & McGlynn, B. L. (2016). Variability in isotopic composition of base flow in two headwater streams of the southern Appalachians. *Water Resources Research*, *52*, 4264–4279. https://doi.org/10.1002/2015wr018463

Soulsby, C., Malcolm, R., Helliwell, R., Ferrier, R. C., & Jenkins, A. (2000). Isotope hydrology of the Allt a' Mharcaidh catchment, Cairngorms, Scotland: Implications for hydrological pathways and residence times. *Hydrological Processes*, *14*(4), 747–762. https://doi.org/10.1002/(SICI)1099-1085(200003)14:4<747::AID-HYP970>3.0.CO;2-0

Spies, T. (2016). LiDAR data (August 2008) for the Andrews Experimental Forest and Willamette National Forest study areas. Long-Term Ecological Research. Forest Science Data Bank, Corvallis, OR. [Database]. Available: http://andlter.forestry.oregonstate.edu/data/abstract.aspx?dbcode=GI010 (26 January 2015). https://doi.org/10.6073/pasta/c47128d6c63dff39ee48604ecc6fabfc

Steel, E. A., Sowder, C., & Peterson, E. E. (2016). Spatial and temporal variation of water temperature regimes on the Snoqualmie River network. *Journal of the American Water Resources Association*, *52*(3), 769–787. https://doi.org/10.1111/1752-1688.12423

Swanson, F., & James, M. (1975). Geology and geomorphology of the H.J. Andrews Experimental Forest, western Cascades, Oregon. Res. Pap. PNW-188. Retrieved from Portland, OR.

Swanson, F. J. (2005). Upper Blue River geology clipped to the Andrews Experimental Forest, 1991. Long-Term Ecological Research. Forest Science Data Bank, Corvallis, OR. [Database]. Available: http://andlter.forestry.oregonstate.edu/data/abstract.aspx?dbcode=GE009 (12 November 2018) https://doi.org/10.6073/pasta/1c428e8798a2f3975f202636d3ad6139

Swanson, F. J. (2013). Mass movement assessment: Cascade hazards ratings, Andrews Experimental Forest, 1992. Long-Term Ecological Research. Forest Science Data Bank, Corvallis, OR. [Database]. Available: http://andlter.forestry.oregonstate.edu/data/abstract.aspx?dbcode=GE010

Swanson, F. J., & Jones, J. A. (2002). Geomorphology and hydrology of the HJ Andrews experimental forest, Blue River, Oregon. *Field Guide to Geologic Processes in Cascadia*, 289–313.

Swanson, F. J., & Swanston, D. N. (1977). Complex mass-movement terrains in the western Cascade Range, Oregon. In D. R. Coates (Ed.), *Landslides*. Reviews in Engineering Geology.Geological Society of America, 3, 113–124. https://doi.org/10.1130/REG3-p113

Tague, C., & Grant, G. E. (2004). A geological framework for interpreting the low-flow regimes of Cascade streams, Willamette River Basin, Oregon. *Water Resources Research*, *40*, W04303. https://doi.org/10.1029/2003WR002629

Tague, C., & Grant, G. E. (2009). Groundwater dynamics mediate low-flow response to global warming in snow-dominated alpine regions. *Water Resources Research*, *45*, W07421. https://doi.org/10.1029/2008WR007179

Taskey, R. D., Harward, M. E., & Youngberg, C. T. (1978). Relationship of clay mineralogy to landscape stability. In C. T. Youngberg (Ed.), *Forest Soils and Land Use: Proceedings of the Fifth North American Forest Soils Conference held at Colorado State University* (p. 140–164). Fort Collins: Dept. of Forest and Wood Sciences, Colorado State University.

Tetzlaff, D., Seibert, J., McGuire, K. J., Laudon, H., Burns, D. A., Dunn, S. M., & Soulsby, C. (2009). How does landscape structure influence catchment transit time across different geomorphic provinces? *Hydrological Processes*, *23*(6), 945–953. https://doi.org/10.1002/hyp.7240

Tetzlaff, D., & Soulsby, C. (2008). Sources of baseflow in larger catchments-Using tracers to develop a holistic understanding of runoff generation. *Journal of Hydrology*, *359*(3-4), 287–302. https://doi.org/10.1016/j.jhydrol.2008.07.008

Verfaillie, D., Lafaysse, M., Déqué, M., Eckert, N., Lejeune, Y., & Morin, S. (2018). Multi-component ensembles of future meteorological and natural snow conditions for 1500 m altitude in the Chartreuse mountain range, Northern French Alps. *The Cryosphere*, *12*(4), 1249–1271. https://doi.org/10.5194/tc-12-1249-2018

ver Hoef, J., Peterson, E., Clifford, D., & Shah, R. (2014). SSN: An R package for spatial statistical modeling on stream networks. *56*(3), 45. https://doi.org/10.18637/jss.v056.i03

ver Hoef, J. M., & Peterson, E. E. (2010). A moving average approach for spatial statistical models of stream networks. *Journal of the American Statistical Association*, *105*(489), 6–18. https://doi.org/10.1198/jasa.2009.ap08248

Vespasiano, G., Apollaro, C., de Rosa, R., Muto, F., Larosa, S., Fiebig, J., et al. (2015). The Small Spring Method (SSM) for the definition of stable isotope-elevation relationships in Northern Calabria (Southern Italy). *Applied Geochemistry*, *63*, 333–346. https://doi.org/10.1016/j.apgeochem.2015.10.001

Walker, G. W., & MacLeod, N. S. (1991). Geologic map of Oregon. U. S. Geological Survey, scale 1:500,000, 2 sheets. U. S. Geological Survey

Wassenaar, L. I., Athanasopoulos, P., & Hendry, M. J. (2011). Isotope hydrology of precipitation, surface and ground waters in the Okanagan Valley, British Columbia, Canada. *Journal of Hydrology*, *411*(1–2), 37–48. https://doi.org/10.1016/j.jhydrol.2011.09.032

Wassenaar, L. I., van Wilgenburg, S. L., Larson, K., & Hobson, K. A. (2009). A groundwater isoscape (δD, δ18O) for Mexico. *Journal of Geochemical Exploration*, *102*(3), 123–136. https://doi.org/10.1016/j.gexplo.2009.01.001

Williams, A. E., & Rodoni, D. P. (1997). Regional isotope effects and application to hydrologic investigations in southwestern California. *Water Resources Research*, *33*(7), 1721–1729. https://doi.org/10.1029/97WR01035

Woods, R. A., Sivapalan, M., & Robinson, J. S. (1997). Modeling the spatial variability of subsurface runoff using a topographic index. *Water Resources Research*, *33*(5), 1061–1073. https://doi.org/10.1029/97WR00232

Yonge, C. J., Goldenberg, L., & Krouse, H. R. (1989). An isotope study of water bodies along a traverse of southwestern Canada. *Journal of Hydrology*, *106*(3), 245–255. https://doi.org/10.1016/0022-1694(89)90075-9

Zimmer, M. A., & Gannon, J. P. (2018). Run-off processes from mountains to foothills: The role of soil stratigraphy and structure in influencing run-off characteristics across high to low relief landscapes. *Hydrological Processes*, *32*(11), 1546–1560. https://doi.org/10.1002/hyp.11488

Zuecco, G., Penna, D., & Borga, M. (2018). Runoff generation in mountain catchments: Long-term hydrological monitoring in the Rio Vauz catchment, Italy. *Cuadernos De Investigacion Geografica*, *44*(2), 397–428. https://doi.org/10.18172/cig.3327